Available at: http://www.ictp.trieste.it/~pub_off IC/2002/148

United Nations Educational Scientific and Cultural Organization
and
International Atomic Energy Agency

THE ABDUS SALAM INTERNATIONAL CENTRE FOR THEORETICAL PHYSICS

REALISTIC MODELLING OF THE SEISMIC INPUT: SITE EFFECTS AND PARAMETRIC STUDIES

F. Romanelli[1]
Department of Earth Sciences, University of Trieste,
Via Weiss 4, Trieste, Italy

F. Vaccari and G. F. Panza
Department of Earth Sciences, University of Trieste,
Via Weiss 4, Trieste, Italy
and
The Abdus Salam International Centre for Theoretical Physics, SAND Group,
Trieste, Italy.

MIRAMARE - TRIESTE

November 2002

[1] Corresponding author: Tel: +39-040-5582116; Fax: +39-040-5582111; E-mail: romanel@dst.univ.trieste.it

ABSTRACT

We illustrate the work done in the framework of a large international cooperation, showing the very recent numerical experiments carried out within the framework of the EC project “Advanced methods for assessing the seismic vulnerability of existing motorway bridges” (VAB) to assess the importance of non-synchronous seismic excitation of long structures. The definition of the seismic input at the Warth bridge site, i.e. the determination of the seismic ground motion due to an earthquake with a given magnitude and epicentral distance from the site, has been done following a theoretical approach. In order to perform an accurate and realistic estimate of site effects and of differential motion it is necessary to make a parametric study that takes into account the complex combination of the source and propagation parameters, in realistic geological structures. The computation of a wide set of time histories and spectral information, corresponding to possible seismotectonic scenarios for different sources and structural models, allows us the construction of damage scenarios that are out of the reach of stochastic models, at a very low cost/benefit ratio.

1. Introduction

It is well accepted that one of the most important factors influencing the space variability of the ground motion is the site response. The local amplification, or de-amplification, effects can dominate the ground-shaking response whenever severe lateral heterogeneities are present in the vicinity of a site. In presence of lateral heterogeneities, like topographic features and/or soft sedimentary basins, the insurgence of local surface waves and local resonances can give rise to a complicated pattern in the spatial ground-shaking scenario, down to a length scale comparable with the smallest wavelength contained in the seismic wave train. If an extended built structure has dimensions greater than the characteristic wavelength of the ground motion, different parts of its foundations can vibrate out of phase due to a non-synchronous seismic input. The whole structure does not move in a coherent way with the surrounding ground, being differential motion relevant. For very extended-in-plan structure (e.g. pipelines, bridges), the differential motion can play an important role also when no strong lateral heterogeneities are present in the vicinity. In fact the so-called wave-passage effect (i.e. the phase shift of the seismic arrivals at the different parts of the structure) is sufficient to generate incoherent motion on a scale length of the order of one hundred meters.

Commonly in the engineering analysis practice, a stochastic model is adopted for the spatial variability of the ground motion, describing the out-of-phase effects in terms of so-called coherency functions. The limitation of such an approach is that the incoherence effect, the wave-passage effect and the local effect are described separately by statistical spectral models that are stationary in time and homogeneous in space. The final result of such an approach implies to resort to convolutive methods, whose low reliability has been discussed in detail for example by [1,2,3].

A better understanding of the ground motion spatial variability can be obtained installing local, dense, seismic arrays at different sites. This implies the recording, with a network of instruments, of multiple seismic sources. The cost of such an operation is evident. The theoretical approach, based on the computation of synthetic seismograms, for the estimation of the site responses uses computer codes, developed from a detailed knowledge of the seismic source process and of the propagation of seismic waves, that can simulate the ground motion associated with the given earthquake scenario. In such a way, synthetic signals, to be used as seismic input in a subsequent engineering analysis, e.g. for the design of earthquake-resistant structures or for the estimation of differential motion, can be produced at a very low cost/benefit ratio. The availability of reliable data about the geometry and mechanical properties of the medium, and about the seismic sources, is in general assured by the

preliminary studies that are required for the construction of important structures and therefore the deterministic calculations of ground motion are possible.

The realistic modeling of ground motion requires the simultaneous knowledge of the geotechnical, lithological, geophysical parameters and topography of the medium, on one side, and tectonic, historical, paleoseismological, seismotectonic models, on the other, for the best possible definition of the probable seismic source. The initial stage of the work was thus devoted to the collection of all available data concerning the deep and shallow geology, the construction of cross-sections along which to model the ground motion, and the specification of the possible seismic sources. Following the upgrade and the improvement of the initial databank of seismic sources (i.e. focal mechanisms) and structural (i.e. bedrock and local) models, the seismic input calculation has been performed at different stages and adopting a set of possible scenarios for the seismic source - Warth bridge configurations.

2. Definition of bedrock and local structural models

The regional structural model for the area where the Warth site lies is adapted from the I-dataset [4]. The vertical dependence of the elastic and anelastic parameters is shown in Figure 1. Starting from the available Warth bridge section plan, a digitized model of the geological cross-section underlying the bridge has been assembled (see Figure 2a). On the basis of the geological and geotechnical information available and considering the results obtained from a local refraction seismic survey, the elastic and the anelastic parameters (see Table 1) have been assigned to the various polygons, corresponding to the different geotechnical units, contained in the section (see Figure 2).

3. Definition of source models: first parametric study

To define the possible seismic sources that control the seismic hazard of the Warth region, we used the available database of focal mechanisms [5]. Taking into account the magnitudes and the epicentral distances from the Warth region, we initially selected the five sources, whose focal mechanism parameters are listed in Table 2, shown in Figure 3.

The distances of the selected sources from the Warth bridge site (assumed geographical coordinates Latitude=47.660ºN and Longitude=16.170ºE) are respectively 41.2 km, 20.3 km, 26.8 km, 8.6 km and 13.7 km. As a conservative choice, magnitude (5.5) and hypocentral depth (5 km) have been kept constant for all the sources, and the source finiteness has been taken into account by properly weighting the source spectrum using the scaling laws of [6], as reported in [7]. The synthetic seismograms at the base of each pier (displacements, velocities and accelerations for the

radial, transverse and vertical components) have been computed, with cut-off frequency at 10 Hz, using the bedrock model. From the analysis of the results, in time (amplitude and duration) and frequency domain, we obtain that source SEE72 (see Table 2) is the most interesting from the seismic hazard assessment point of view. Therefore SEE72 has been used for the preliminary computation of the seismic input at the Warth bridge site.

We have performed a parametric study of the ground motion in order to take into account the variations due to the choice of the focal mechanism parameters. Varying the geometry of the seismic source, different ground motions at the Warth site have been studied, in order to reach the maximum excitation in both longitudinal and transverse direction. Starting from the Maximum Historical Earthquake, an additional study has been made considering the magnitude corresponding to both the Maximum Credible Earthquake and the Maximum Design Earthquake.

Starting from source model SEE72, in the first three tests the source depth is fixed at 5 km (as a conservative choice) while the distance to the bridge is 8.6 km. The strike has been varied from 0° to 360° (see Figure 4), the dip from 0° to 90° (see Figure 5) and the rake from 0° to 180° (see Figure 6). For every test, displacement, velocity and acceleration are computed assuming the other angles fixed at the values shown in Table 2.

For a more general study, three other tests have been performed: the dip angle has been fixed at 45°, 70° and 90° varying the strike and the rake (e.g. see Figure 7). Once established the most effective combination for the transverse and the radial components of motion (strike=60°, dip=70°,rake=0, 90° for transverse and radial components respectively), in the last test the source depth (from 1 to 20 km) and the epicentral distance (from 5 to 20 km) have been varied (see Figure 8). The results shown in Figure 6 allow us to conclude that, for a fixed magnitude, the most effective focal depth, for an epicentral distance of 8-9 km, is 6 km both for the transverse (Figure 8a) and the radial (Figure 8b) components of motion (the focal depths between 1 and 3 km are shown for completeness but they are highly unrealistic).

The most effective focal mechanisms in radiating SH waves (transverse component) and P-SV waves (radial and vertical component), propagating towards the Warth bridge in the adopted structural model are listed in Table 3.

4. Definition of the seismic input: results from the first parametric study

To deal both with realistic source and structural models, including topographical features, a hybrid method has been developed that combines modal summation and the finite difference technique (e.g. [8,9]), and optimizes the use of the advantages of both methods. Wave propagation is treated

by means of the modal summation technique from the source to the vicinity of the local, heterogeneous structure that we may want to model in detail. A laterally homogeneous anelastic structural model is adopted, that represents the average crustal properties of the region. The generated wavefield is then introduced in the grid that defines the heterogeneous area and it is propagated according to the finite differences scheme (see Figure 9). With this approach, source, path and site effects are all taken into account, therefore a detailed study of the wavefield that propagates even at large distances from the epicenter, without having to resort to convolutive methods, that may be quite misleading (e.g. [1,2,3]), is possible.

In the hybrid scheme the local heterogeneous model shown in Figure 3c has been coupled with the average regional model used in the initial analysis (see Figure 1). The minimum S-wave velocity in the model is 220 m/s, and the mesh used for the finite differences is defined with a grid spacing of 3 m. This allows us to carry out the computations at frequencies as high as about 8 Hz, well above the frequency range relevant for large dimensions objects, like Warth bridge.

The synthetic time signals (displacements, velocities and accelerations) have been calculated for the three components of motion. The working magnitude is 5.5 (seismic moment equal to 1.8 10^{17}Nm), corresponding to the nearest largest recorded event, but the magnitude range 5.0-6.0 has been explored. The study of possible directivity effects in the direction of the Warth cross section has been performed adopting a new method, based on the modeling of a Haskell-type [10,11] source. A stochastic component allows us to build a spectrum (amplitude and phase) of the source function that takes into account both the rupture process and directivity effects. As an example the transverse acceleration time series, calculated at the bridge piers, with the two methods (scaled point source [6] and Haskell-type source), are plotted in Figure 10a while in Figure 10b the corresponding Fourier amplitude spectra are shown. Figure 11 shows the same results for the radial component of motion.

We give an estimate of the local response at each site, evaluating the Spectral Ratios, using both the Fourier Spectra (FSR) and the Response Spectra (RSR), corresponding to the laterally varying model and to the reference bedrock model. As an example, the response spectra for the signals (Haskell-type source) of Figure 10a and 11a, and the corresponding RSR and FSR, are shown in Figures 12 and 13n respectively. In Figure 14, the RSR versus epicentral distance and frequency are shown for transverse and radial components of motion, together with the results of the radial/vertical (henceforth named H/V) RSR.

5. Definition of source models: second parametric study

The seismic energy of the accelerograms shown in Figures 10 and 11 exhibits the greatest peaks in the frequency range from 3 to 6 Hz, reaching considerable peak values (around 0.4 g). Another parametric study has been performed in order to find a seismic source-Warth site configuration providing a set of signals whose seismic energy is concentrated around 1 Hz, frequency that corresponds approximately to that of the fundamental transverse mode of oscillation of the bridge.

The computation of synthetic seismograms (accelerations for the transverse component) has been carried out considering the source SEE-SH buried in the bedrock model. The focal depth and the epicentral distance have been varied in the range 5-20 km and 5-100 km, respectively. The results of Figure 15 show that a relevant value of PGA (e.g. greater than 0.1g) in the period range of interest (0.8-1.2 s) can be reached by a, geophysically sound, source 12 km deep at an epicentral distance of 30 km.

6. Definition of the seismic input: results from the second parametric study

The same computations and analysis described in Section 4, but limited to the transverse component of motion, have been carried out for the configuration defined in Section 5, i.e. strike=60°; dip=70°; rake=0,180°; depth=12km, epicentral distance=30km. In Figure 16 the Fourier amplitude spectra of the acceleration time series calculated for a magnitude equal to 6.0, with and without directivity effects, are shown. The results show that, even if the seismic energy around 1 Hz can be relevant (see bedrock curves), the local structure beneath the Warth bridge greatly amplifies the frequency components between 3 and 7 Hz, i.e. a frequency range not corresponding to the fundamental transverse mode of oscillation of the bridge (about 0.8 Hz). In Figure 17 the RSR versus epicentral distance and frequency are shown.

7. Final definition of the seismic input

In the final set of computations, the local heterogeneous model has been iteratively changed. Initially, the S-wave velocities of the uppermost units (units 1-7 of Figure 2) have been halved (see for comparison Figure 18a and Figure 2); then, in order to characterize the local structure with lower resonant frequencies, some of the geotechnical units have been assigned to a class characterized by lower velocities (unit 7 to unit 4 in Figure 18b; unit 7 and unit 8 to unit 4 in Figure 18c).

The synthetic time series have been computed for the transverse component of motion using the focal mechanism obtained from the parametric studies and the configurations described in Sections 3 and 5:

SS1) Strike=60°; Dip=70°; Rake=0°; Depth=5km; Distance=8km, Magnitude=5.5

SS2) Strike=60°; Dip=70°; Rake=0°; Depth=12km; Distance=30km, Magnitude=6.5

In such a way, using the local models, a, b and c, shown in Figure 18, we obtain six different source-local structure pairs, henceforth named: SS1a; SS1b; SS1c; SS2a; SS2b; SS2c. In Figures 19, 20, 21, 22 and 23 the Fourier amplitude spectra are shown, for the acceleration time series calculated for SS1a, SS1b, SS2b, SS1c and SS2c configurations, respectively. In the model of Figure 18a, only the first two sites have significant resonance at frequencies lower than 3 Hz. Using the model shown in Figure 18b, at the sites from 3 to 6, due to the increased thickness of the layer with S-wave velocity equal to 150 m/s, resonance at lower frequencies, i.e. between 1 and 2 Hz, is visible. Figures 20 and 21 show, as expected, that a deep source excites lower frequencies more than a shallow one, and that the effect of increasing the epicentral distance is to attenuate high frequencies. Similar conclusions may be drawn from Figures 22 and 23, with the difference that, in this case, the frequency peaks appear at significantly lower frequencies. In particular, site 3 is characterized by a peak spectral acceleration (about 0.4 g) very near to the target frequency (i.e. 0.8 Hz). The acceleration time series are shown in Figure 24. In Figures 25, 26, 27, 28 and 29 the RSR versus epicentral distance and frequency are shown for configurations SS1a, SS1b, SS2b, SS1c and SS2c, respectively.

8. Conclusions

Two parametric studies of the ground motion have been performed, taking into account the variations due to the choice of the focal mechanism parameters and the geometry of the seismic source. Different ground motions at the Warth site have been studied in order to define the maximum excitation in longitudinal and transverse direction, which are consistent both with the Maximum Credible Earthquake and with the Maximum Design Earthquake. With the parametric study we have defined a seismic source-Warth site configuration that provides a set of signals whose seismic energy is concentrated around 1 Hz, frequency that corresponds approximately to that of the fundamental transverse mode of oscillation of the bridge. The results have led to the definition of two possible scenarios:

S1) Strike=60°; Dip=70°; Rake=0,180°; Depth=5km; Distance=8km, Magnitude=5.5

S2) Strike=60°; Dip=70°; Rake=0,180°; Depth=12km; Distance=30km, Magnitude=6.5

The analysis of the computed seismic input has been carried out in the time domain (broad band ground motion time series) and in the frequency domain (Fourier and response spectra). We give an estimate of the local response at each site, evaluating the Spectral Ratios, using both the Fourier

Spectra (FSR) and Response Spectra (RSR) for the laterally varying model normalized to the ones computed for the bedrock model.

In the final set of computations, the local heterogeneous model has been iteratively changed, in order to characterize the local structure with lower resonant frequencies. The results obtained with the last variant of the local model, which is characterized by an exaggeratedly thick low velocity layer, show that only in this case the resonant peaks, present at frequencies around 0.8 Hz, are the dominant features of the entire spectra. Therefore the main practical conclusion of our analysis, verified by laboratory experiments carried out at JRC-ISPRA within the VAB Project [12,13], is that the Warth bridge is likely to well stand the most severe seismic input compatible with the seismic regime of the Eastern Alps.

Acknowledgements

The results are part of the studies that are being carried on for the E. C. Environmental Programme RTD Project ENV4-CT98-0717 “Advanced Methods for Assessing the Seismic Vulnerability of Existing Motorway Bridges (VAB Project)”. The international team was made up of seven partners: Arsenal Research, Vienna, Austria; ISMES S.P.A,. Bergamo, Italy; ICTP, Trieste, Italy; UPORTO, Porto, Portugal; CIMNE, Barcelona, Spain; SETRA, Bagneaux, France; JRC-ISPRA, EU.
We used GMT software [13] in the preparation of Figures 1-2.

References

1. Romanelli, F. and Vaccari, F. (1999). "Site response estimation and ground motion spectral scenario in the Catania Area", *J. of Seism.*, **3**, p. 311-326.
2. Field, E.H., the SCEC Phase III Working Group (2000). "Accounting for site effects in probabilistic seismic hazard analyses of Southern California: overview of the SCEC Phase III report", *Bull. Seism. Soc. Am.*, **90**, 6B, p. S1-S31.
3. Panza, G.F., Romanelli, F. and Vaccari, F. (2001). "Seismic wave propagation in laterally heterogeneous anelastic media: theory and applications to the seismic zonation", *Advances in Geophysics*, Academic press, **43**, 1-95.
4. Du, Z. J., A. Michelini and Panza, G.F. (1998). "EurID: a regionalized 3-D seismological model of Europe", *P.E.P.I.*, **105**, 31-62.
5. Suhadolc, P. and Panza, G. F. (1996). "Focal mechanisms and seismogenetic zones", EEC Technical Report, Project CIPA-CT94-0238.
6. Gusev, A. A. (1983). "Descriptive statistical model of earthquake source radiation and its application to an estimation of short period strong motion", *Geophys. J. R. Astron. Soc.* **74**, 787-800.
7. Aki, K. (1987). "Strong motion seismology", in M. Erdik and M. Toksöz (eds) *Strong ground motion seismology*, NATO ASI Series, Series C: Mathematical and Physical Sciences, D. Reidel Publishing Company, Dordrecht, Vol. 204, pp. 3-39.
8. Fäh, D., Iodice, C., Suhadolc, P. and Panza, G.F (1993). "A new method for the realistic estimation of seismic ground motion in megacities: the case of Rome", *Earthquake Spectra*, **9**, 643-668.
9. Fäh, D., Suhadolc, P., Mueller, St. and Panza, G.F. (1994). "A hybrid method for the estimation of ground motion in sedimentary basins: quantitative modeling for Mexico City", *Bull. Seism. Soc. Am.*, **84**, 383-399.
10. Haskell N. A. (1964). "Total energy and energy spectra density of elastic wave radiation from propagating faults", *Bull. Seism. of Soc. Am.*,Vol. **54**, 1811-1841.
11. Haskell N. A. (1966). "Total energy and energy spectral density of elastic wave radiation from propagating faults. 2. A statistical source model", *Bull. Seism. of Soc. Am.*,Vol. **56**, 125-140.
12. Pinto, A., Molina, J. Tsionis, G. (2001). "Cyclic test on a large-scale model of an existing short bridge pier (Warth bridge-Pier A70)", VAB Technical Report, EU-JRC, EUR 19901En, Ispra.
13. Wessel, P., and Smith, W.H.F. (1991). "Free software helps map and display data", *EOS Trans. AGU*, **72**, 441.

Table 1. Elastic and anelastic parameters of the geotechnical units shown in Figure 2.

Unit	Density g/cm^3	P-wave velocity km/s	Q_P	S-wave velocity km/s	Q_S
1	1.5	0.30	40.0	0.20	15.0
2	1.7	0.49	40.0	0.25	15.0
3	2.0	0.70	50.0	0.26	20.0
4	1.8	0.70	50.0	0.29	20.0
5	2.3	0.80	50.0	0.30	20.0
6	2.3	0.80	50.0	0.40	20.0
7	1.8	1.70	50.0	0.50	20.0
8	2.3	2.10	150.0	1.00	60.0
9	2.3	3.00	150.0	1.90	60.0
10	2.2	1.80	100.0	1.10	40.0

Table 2. Focal mechanisms for the five selected sources.

Source id.	Lon E (°)	Lat N (°)	Focal Depth (km)	Strike (°)	Dip (°)	Rake (°)	Magnitude Ms (Mb)
SEM63	16.200	48.030	?	180	20	90	?
SEM64_1	15.920	47.730	3	90	81	311	(4.7)
SEM64_2	15.950	47.850	1	100	70	31	(5.4)
SEE72	16.120	47.730	18	190	70	324	5.5 (4.9)
NEU72	16.020	47.730	19	127	80	190	4.4

Table 3. Focal mechanisms for the selected sources.

Source id.	Focal Depth (km)	Strike (°)	Dip (°)	Rake (°)	Magnitude
SEE72	5	190	70	324	5.5
SEE-SH	5 and 6	60	70	0 and180	5.0; 5.5; 6.0
SEE-PSV	5 and 6	60	70	90 and 270	5.0; 5.5; 6.0

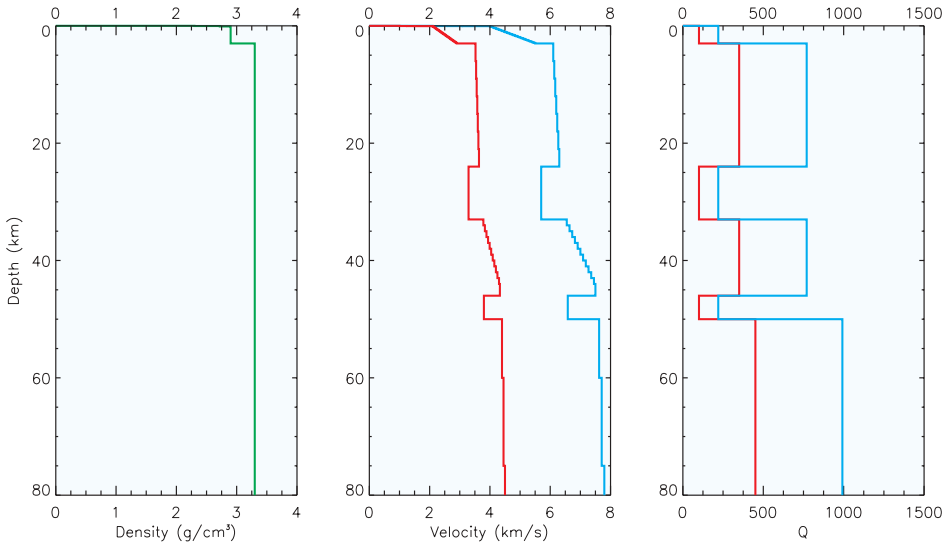

Figure 1. Vertical dependence of the elastic (density, P and S wave velocity) and anelastic (Q_P and Q_S) parameters of the average regional model assumed for the Warth area.

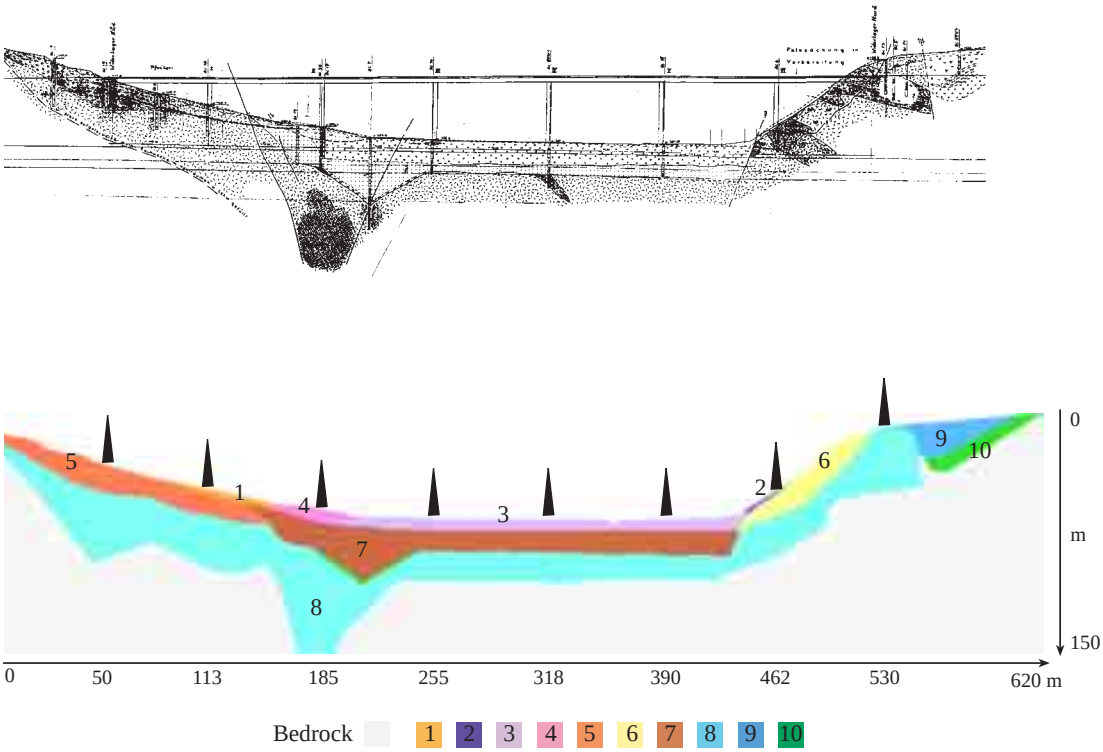

Figure 2. Local heterogeneous model along Warth bridge and its geotechnical units. Black triangles show the sites of the abutments and of the piers and their relative distance along the section.

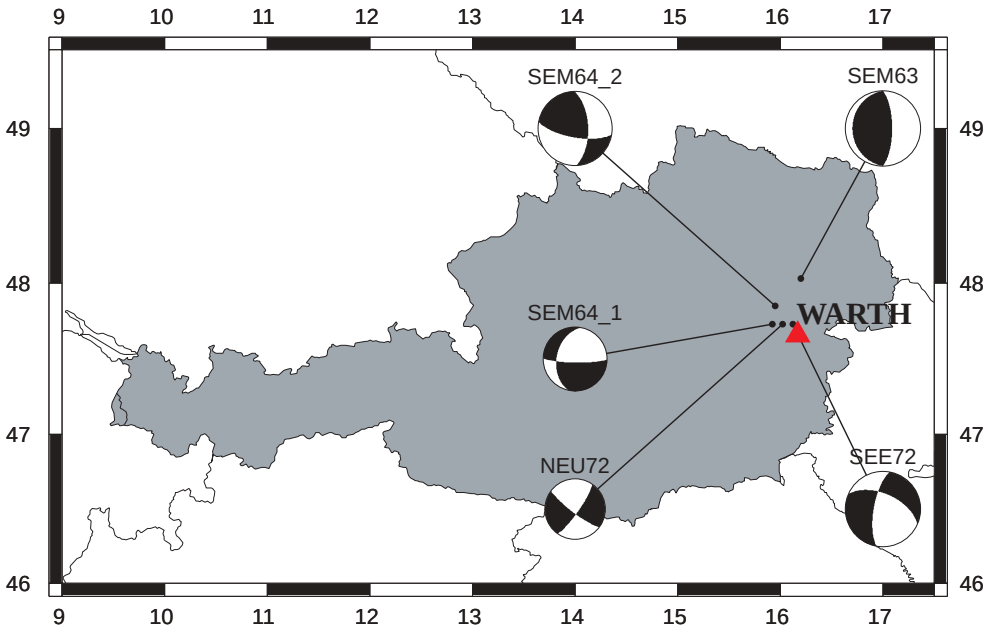

Figure 3. Focal mechanisms of the 5 events reported in Table 2 and Warth site (triangle).

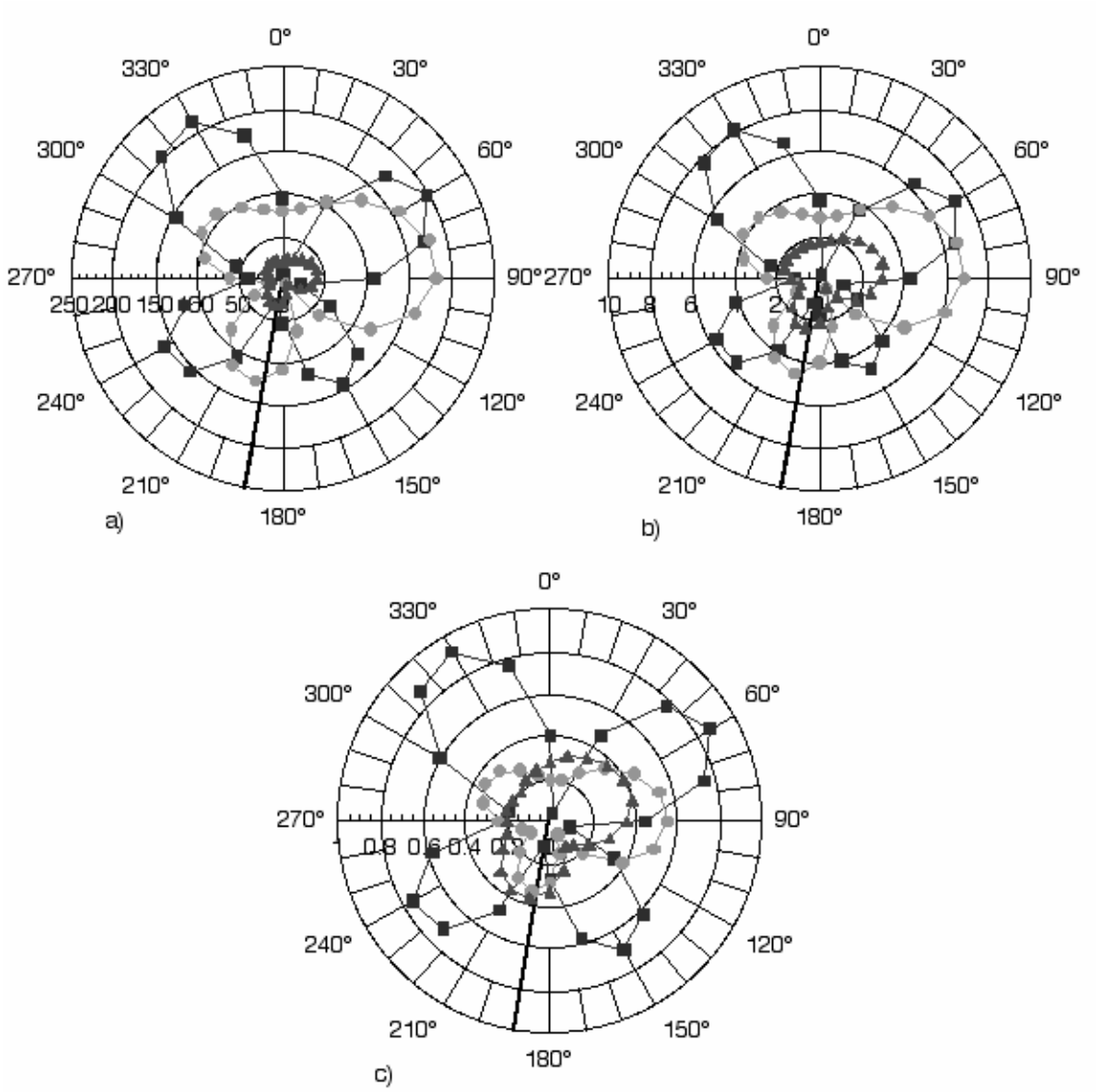

Figure 4. Polar plot of the maximum amplitude of the ground motion – a) acceleration (cm/s^2); b) velocity (cm/s); c) displacement (cm) – versus the strike angle, for the three components – transverse (squares); radial (circles); vertical (triangles). The rake (324°) and dip (70°) angle values are those of mechanism SEE72 reported in Table 2. The thick line represents the case with strike angle (190°).

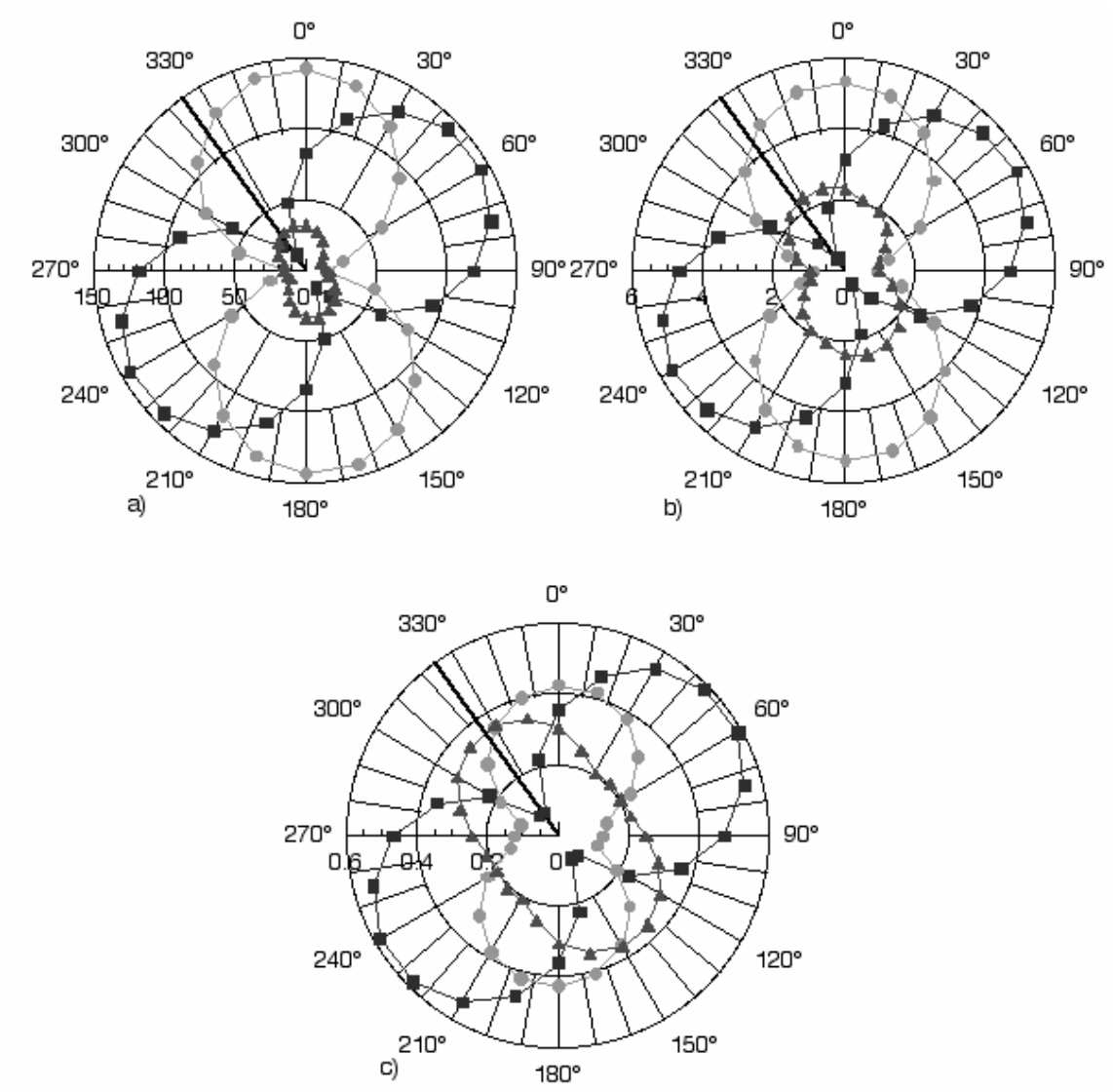

Figure 5. Polar plot of the maximum amplitude of the ground motion – a) acceleration (cm/s^2); b) velocity (cm/s); c) displacement (cm) – versus the rake angle, for the three components – transverse (squares); radial (circles); vertical (triangles). The strike (190°) and dip (70°) angle values are those of mechanism SEE72 reported in Table 2. The thick line represents the case with rake angle (324°).

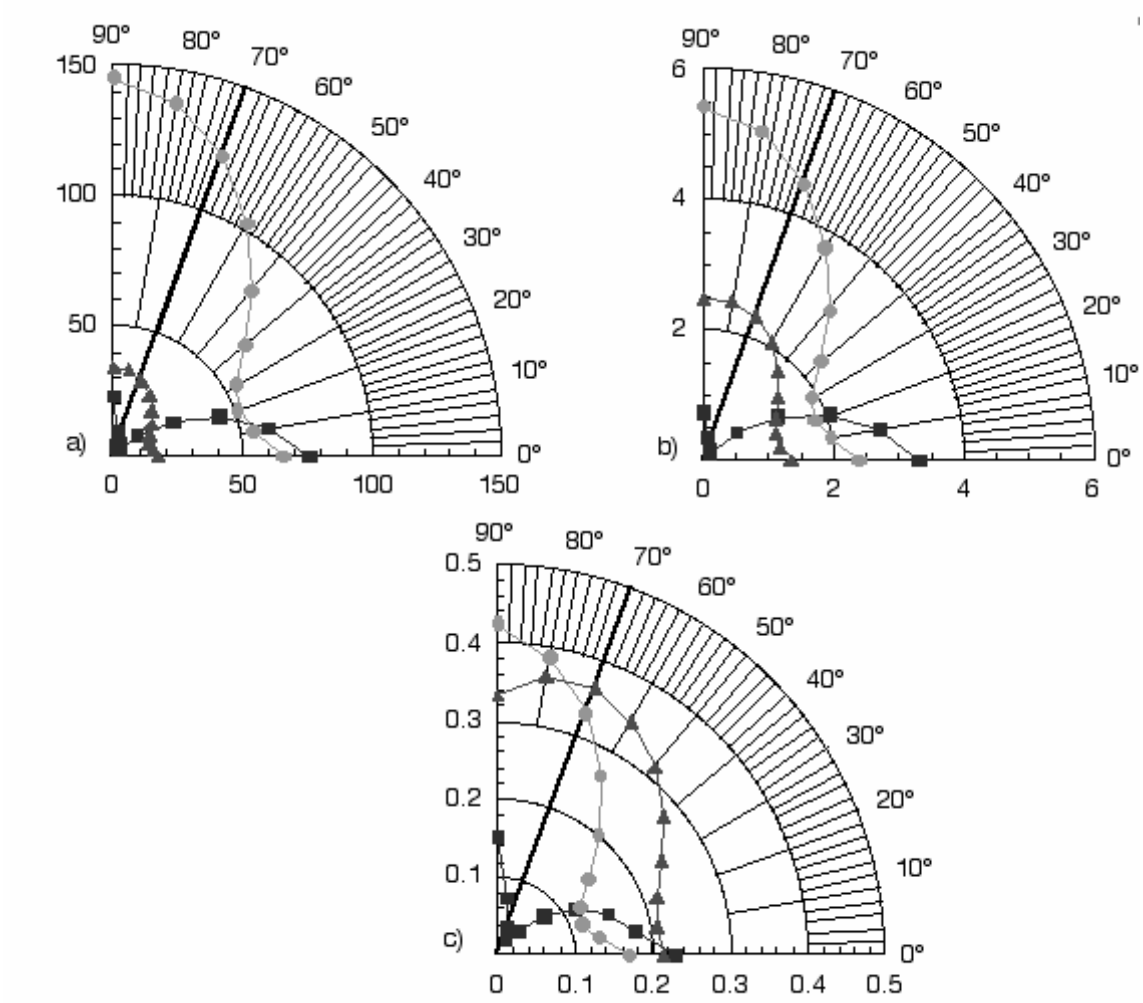

Figure 6. Polar plot of the maximum amplitude of the ground motion – a) acceleration (cm/s^2); b) velocity (cm/s); c) displacement (cm) – versus the dip angle, for the three components – transverse (squares); radial (circles); vertical (triangles). The strike (190°) and rake (324°) angle values are those of mechanism SEE72 reported in Table 2. The thick line represents the case with dip angle (70°).

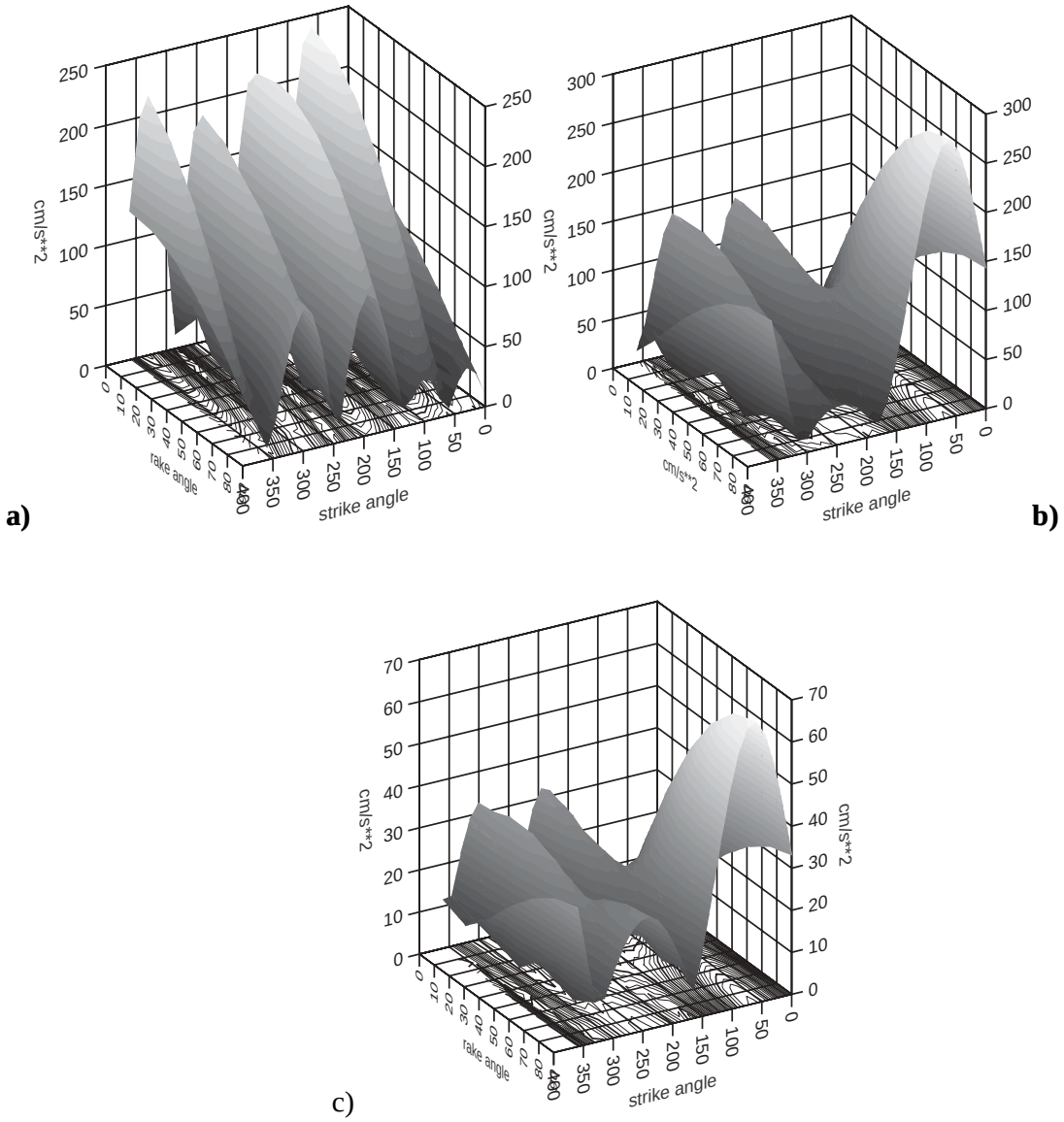

Figure 7. Plot of the maximum amplitude of the ground motion (acceleration) versus the strike and rake angle, for the three components: a) transverse; b) radial; c) vertical. The dip angle is 70°.

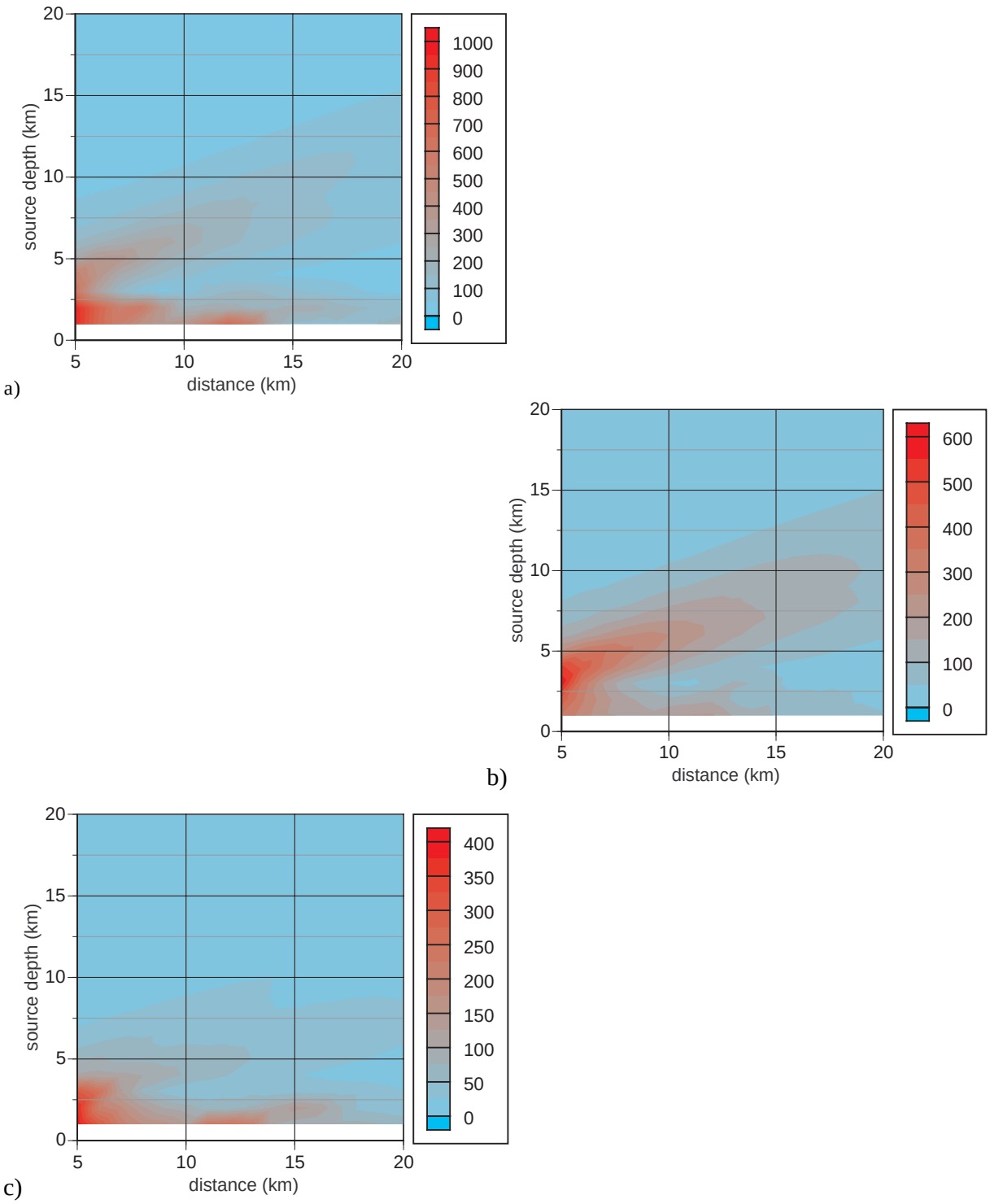

Figure 8. Plot of the maximum amplitude of the ground motion (acceleration – cm/s^2) versus epicentral distance and source depth, for the three components: a) transverse – rake angle=0°; b) radial - rake angle=90°; c) vertical - rake angle=90°, strike=60° and dip=70°.

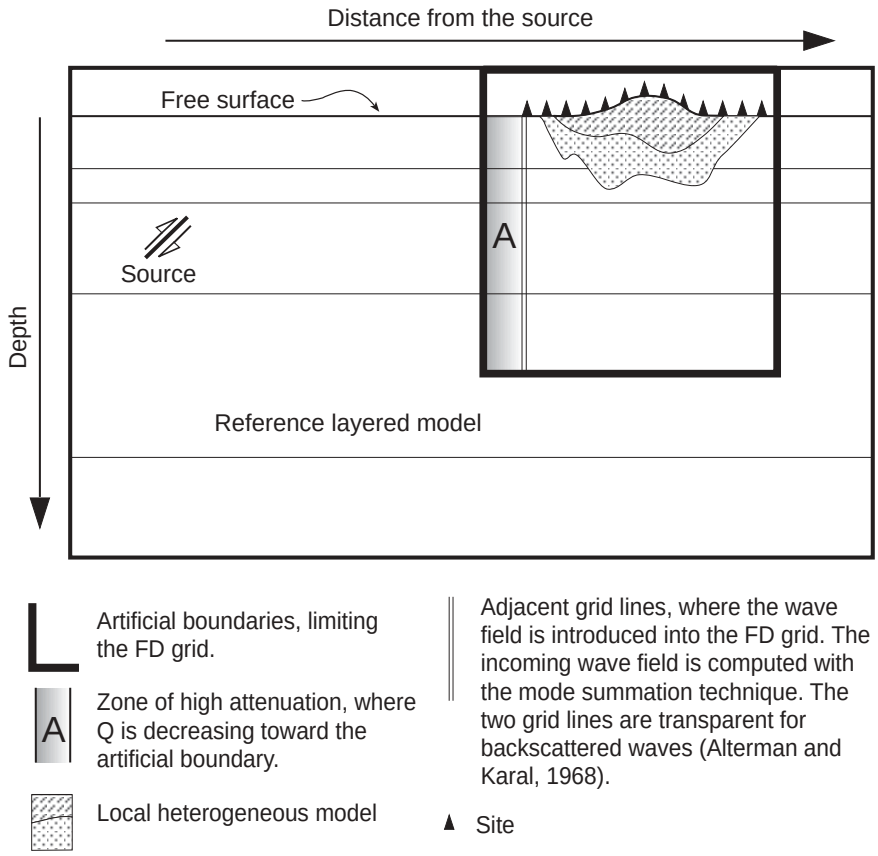

Figure 9. Scheme of the hybrid (modal summation plus finite differences scheme) method (from [3]).

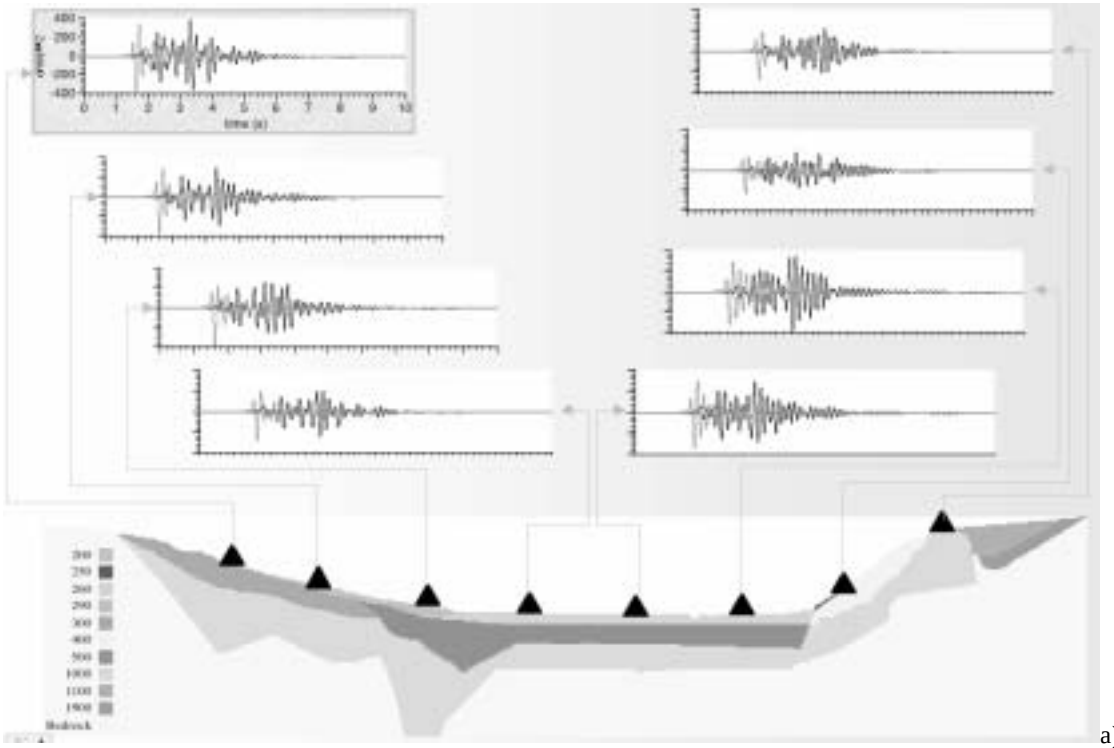

a)

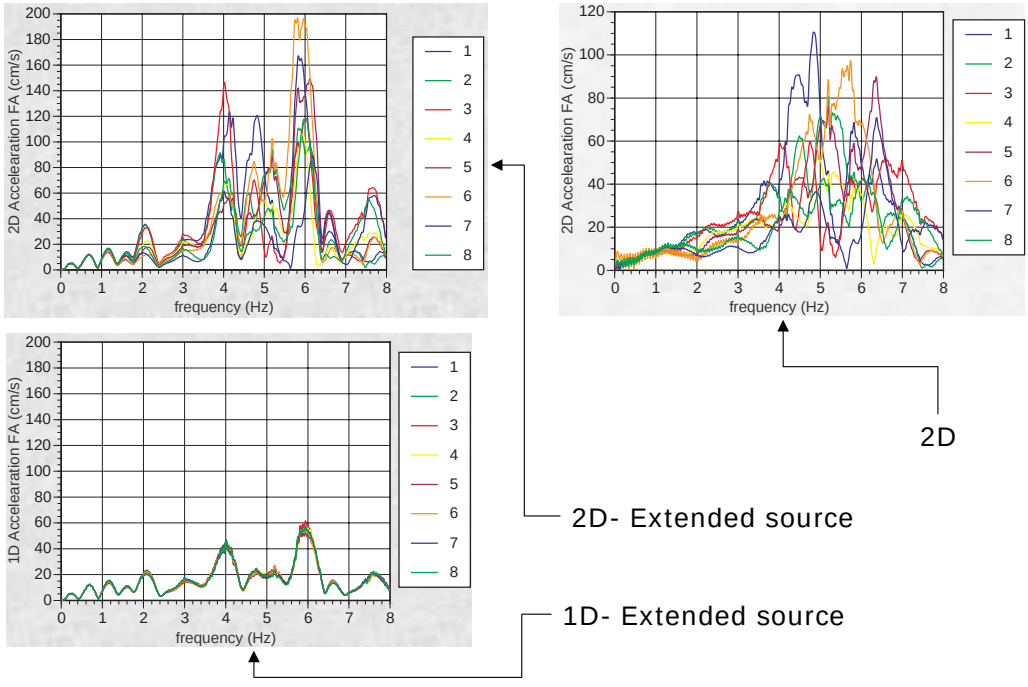

b)

Figure 10. a) Acceleration time series , transverse component and source model SEE-SH, calculated at the position of the bridge piers (plus one at the abutment) , considering the Gusev scaling law for magnitude 5.5 with (blue signals) and without (green signals) directivity effects. b) Fourier amplitude spectra of the signals shown in a), together with those obtained for the bedrock model.

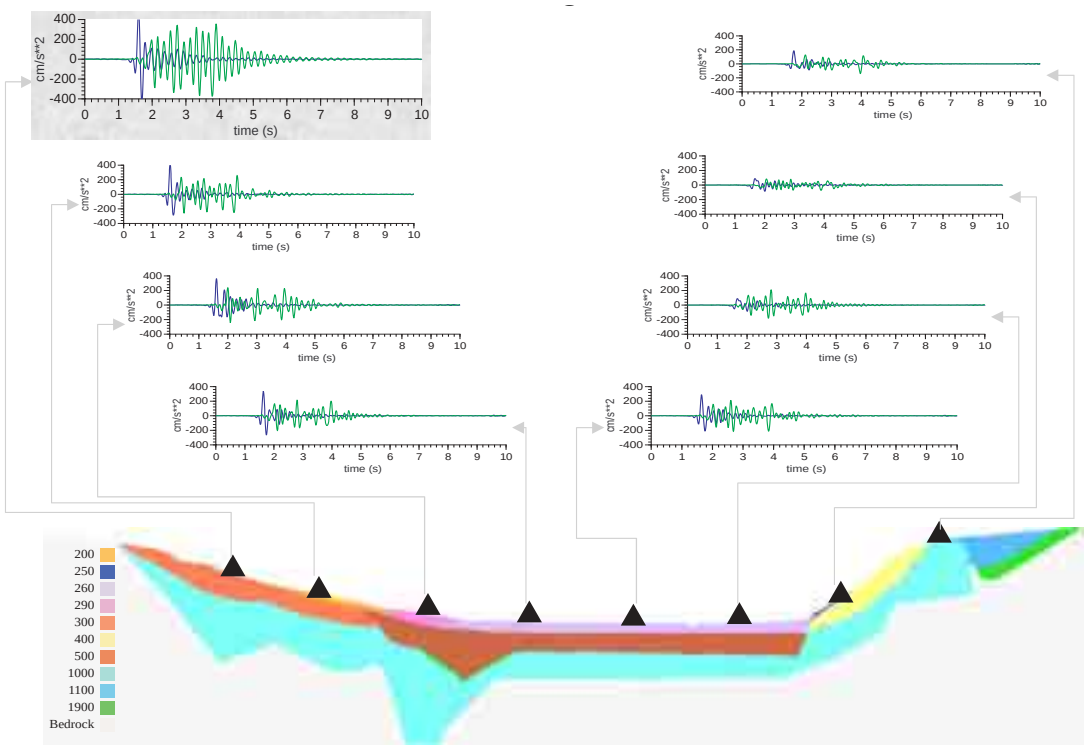

a)

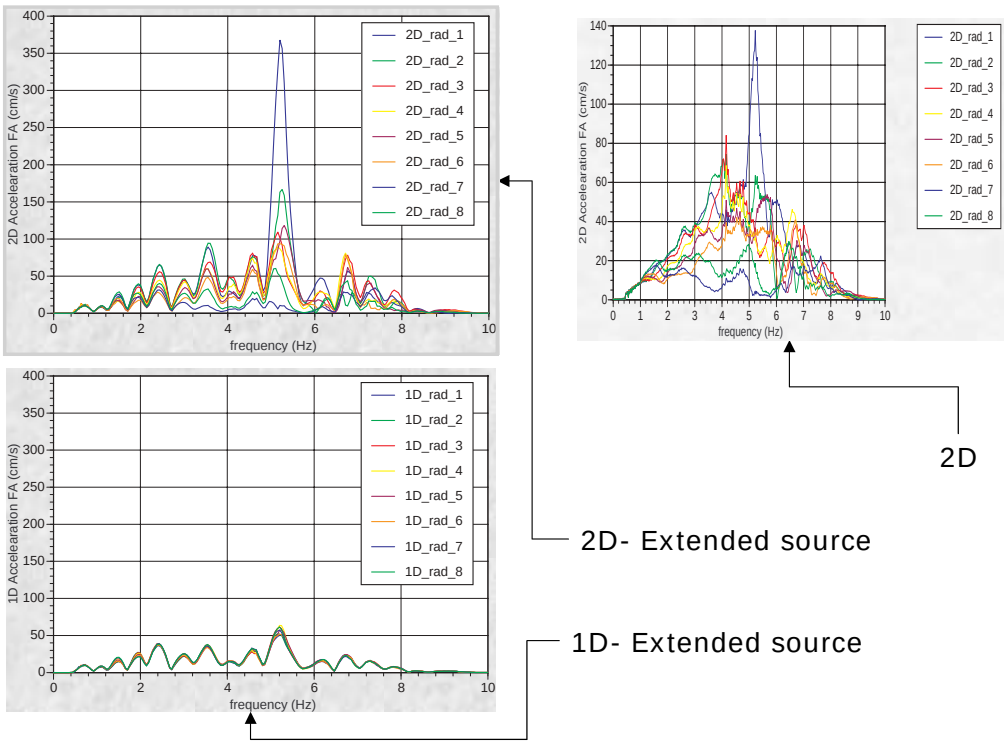

b)

Figure 11. a) Acceleration time series, radial component and source model SEE-PSV, calculated at the position of the bridge piers (plus one at the abutment) , considering the scaling law for magnitude 5.5 with (dark color signals) and without directivity effects. b) Fourier amplitude spectra of the signals shown in a), together with those obtained for the bedrock model .

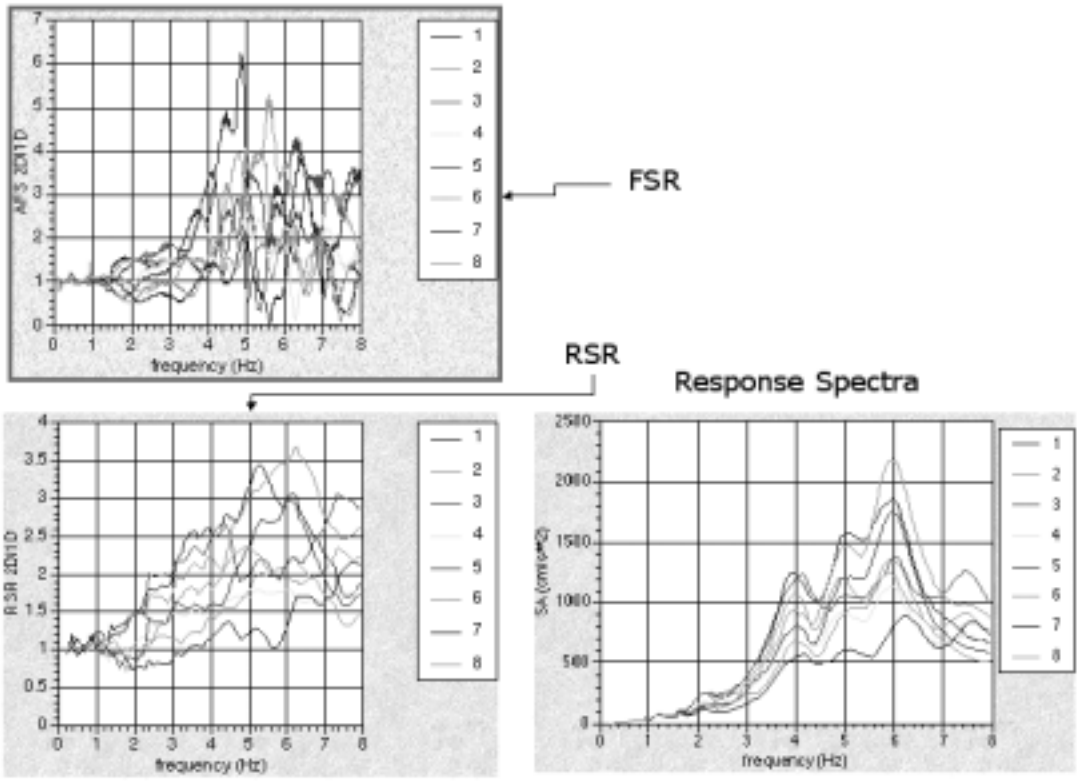

Figure 12. Response spectra for the signals of Figure 10a (Haskell-type source) and the corresponding RSR and FSR.

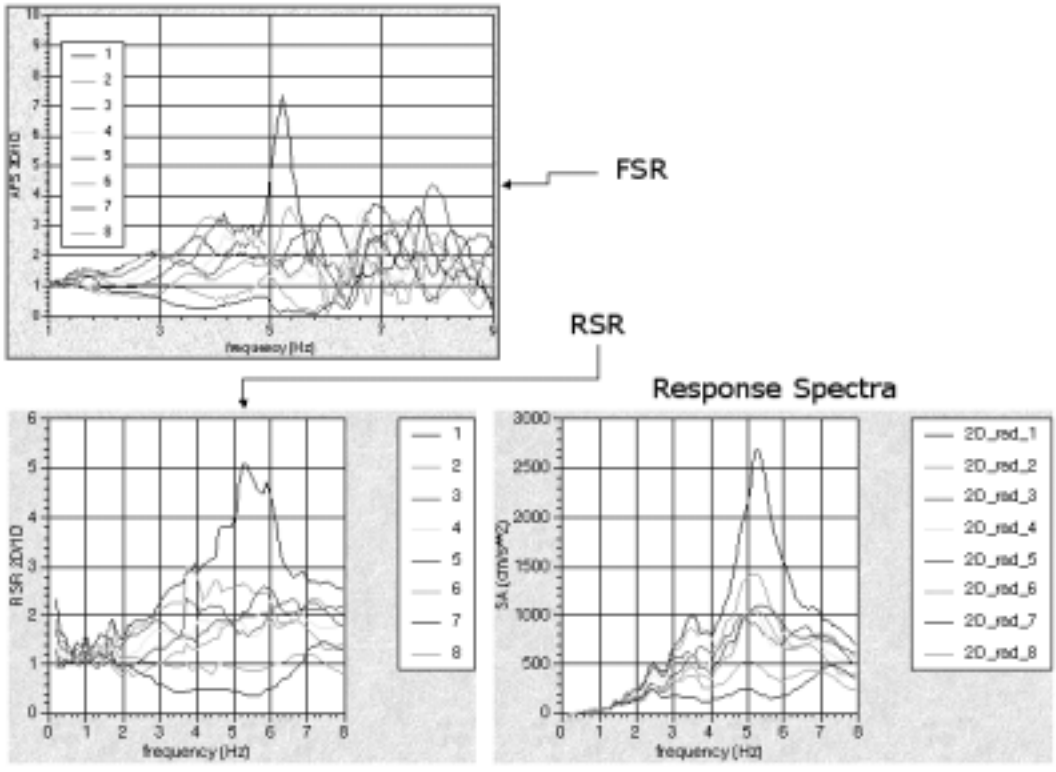

Figure 13. Response spectra for the signals of Figure 11a (Haskell-type source) and the corresponding RSR and FSR.

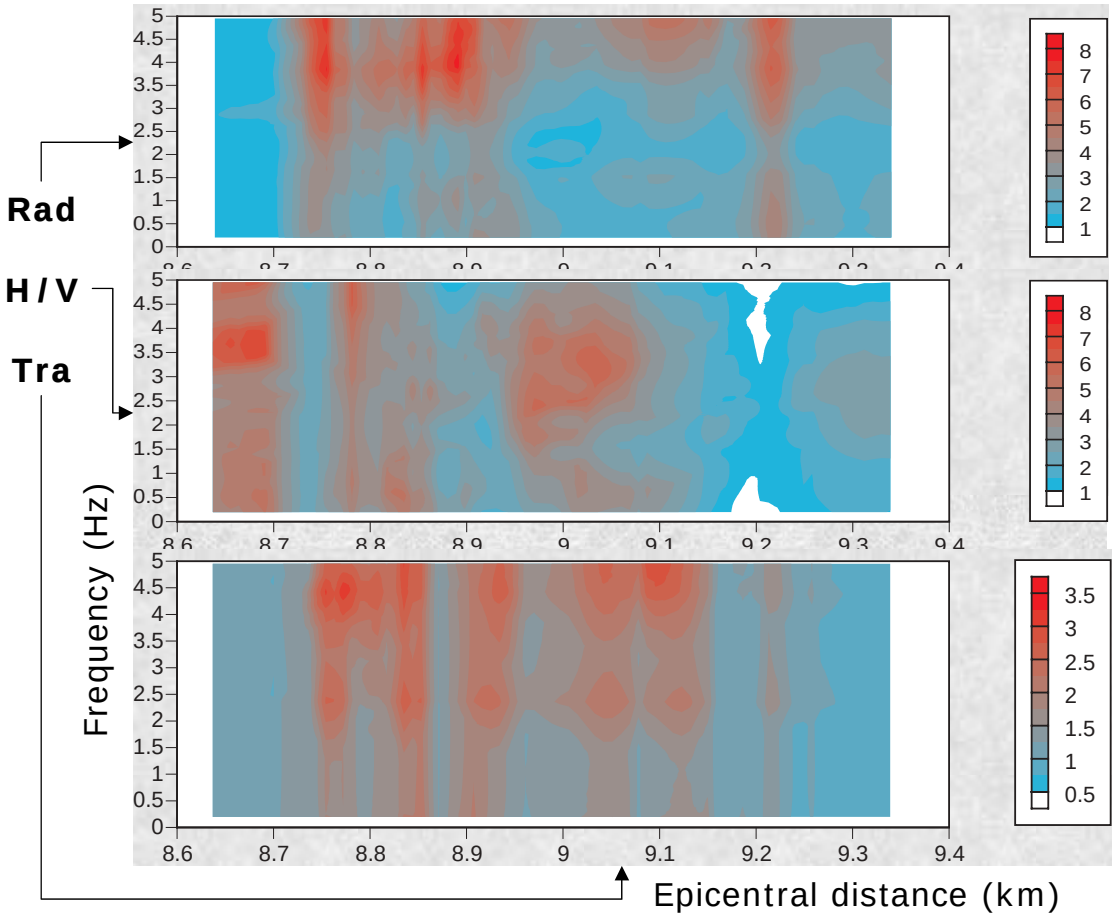

Figure 14. RSR and H / V RSR versus epicentral distance and frequency.

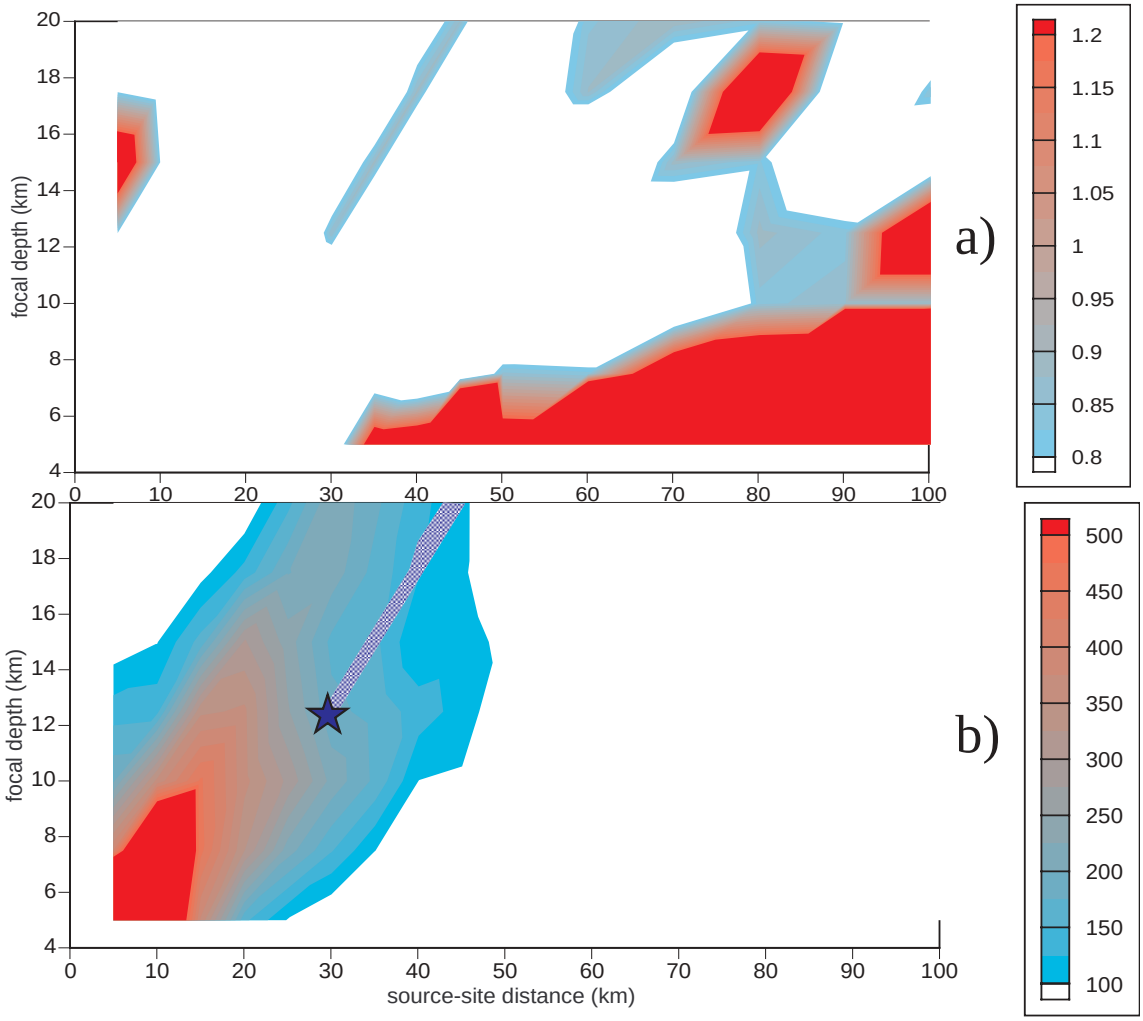

Figure 15. Plot of the period in seconds (a) corresponding to the maximum acceleration in cm/s^2 (b) for the various source depths and site distances configurations that have been tested.

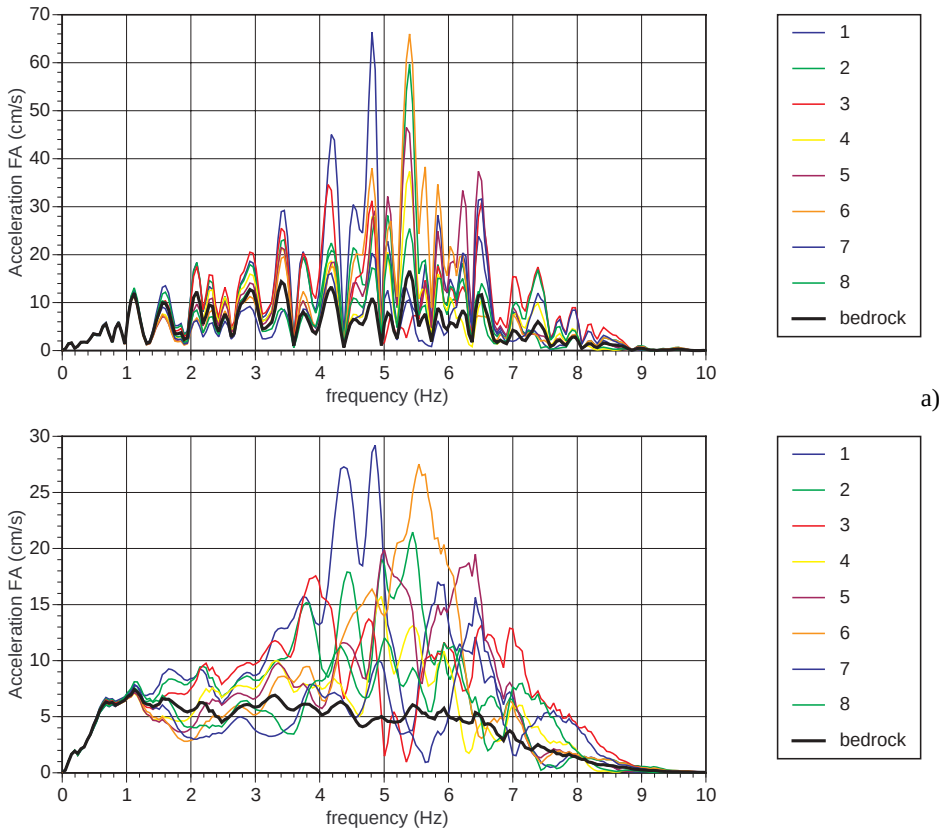

Figure 16. Fourier amplitude spectra of the transverse accelerations calculated at the 8 sites shown in Figure 4a, for a focal depth of 12 km, a source distance of 30 km, a magnitude equal to 6.0, with (a) and without (b) directivity effects. The thick black lines correspond to the curve for the bedrock model (common for all the eight sites).

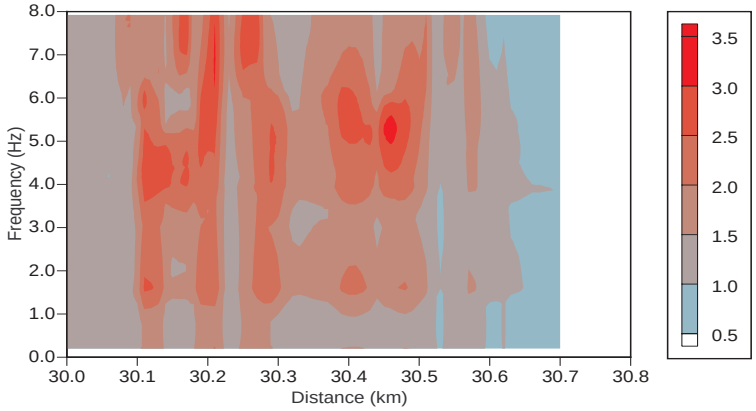

Figure 17. RSR versus epicentral distance and frequency.

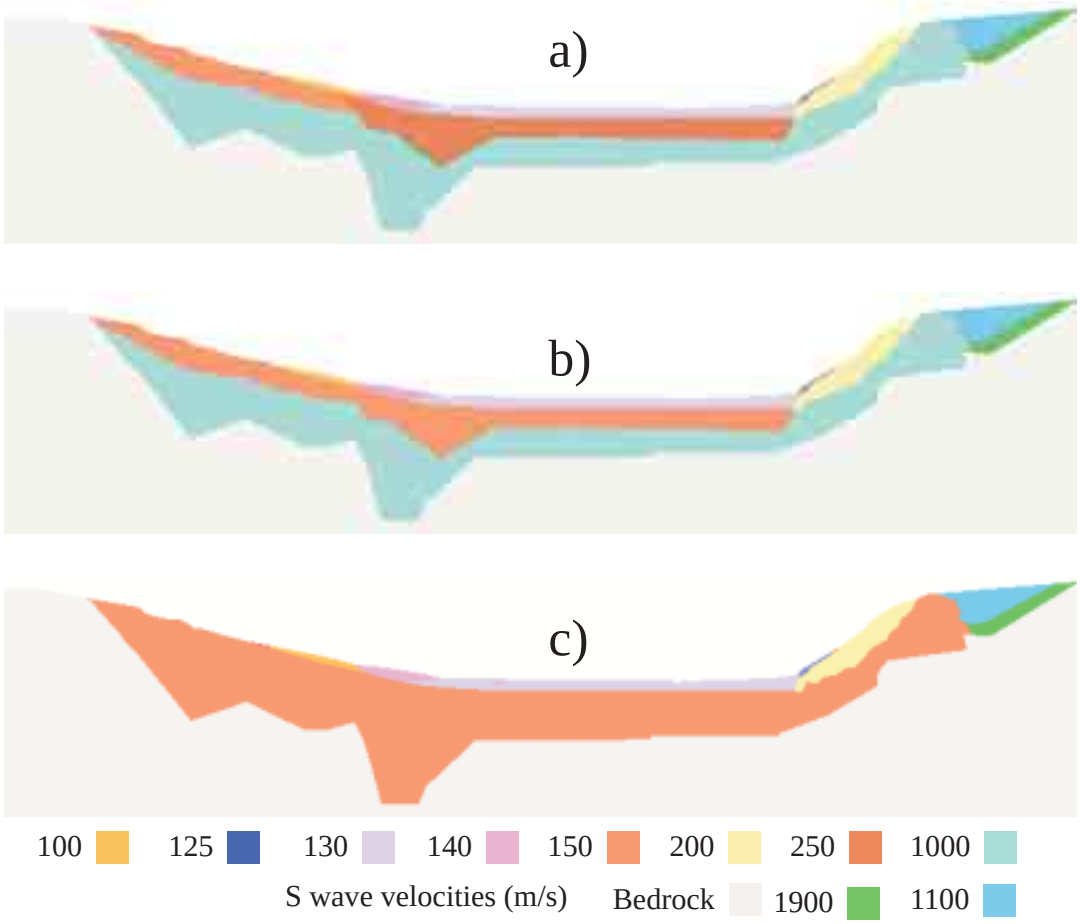

Figure 18. Local geotechnical models of Warth bridge section obtained lowering successively the S-wave velocities of the uppermost units.

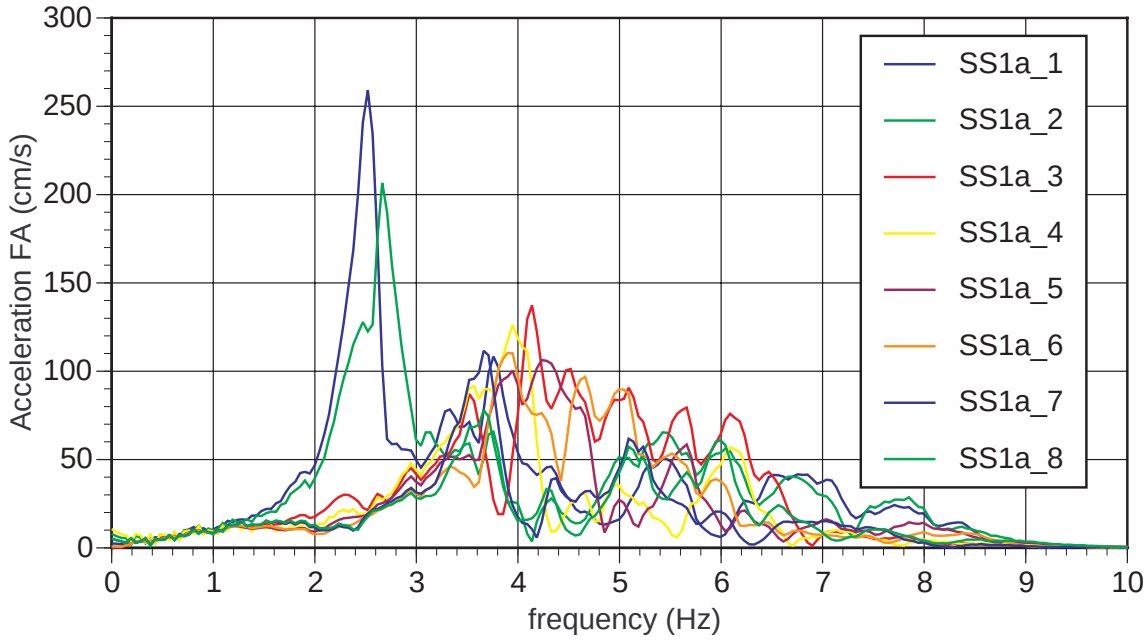

Figure 19. Fourier amplitude spectra of the transverse accelerations calculated at the eight pier sites using the source-section configuration SS1a.

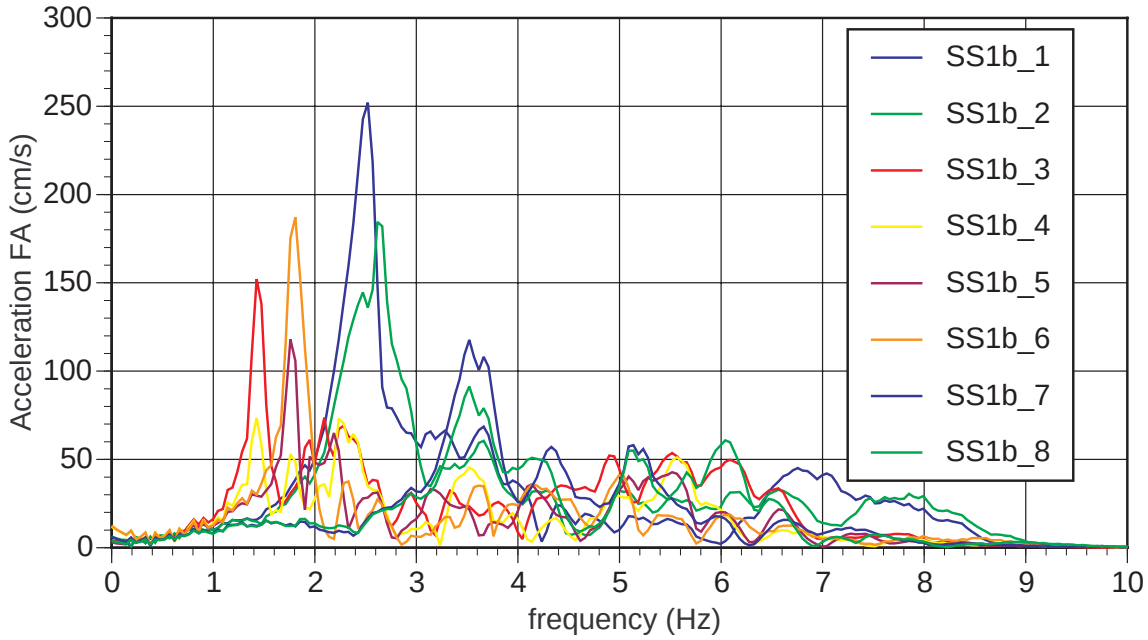

Figure 20. Fourier amplitude spectra of the transverse accelerations calculated at the eight pier sites using the source-section configuration SS1b.

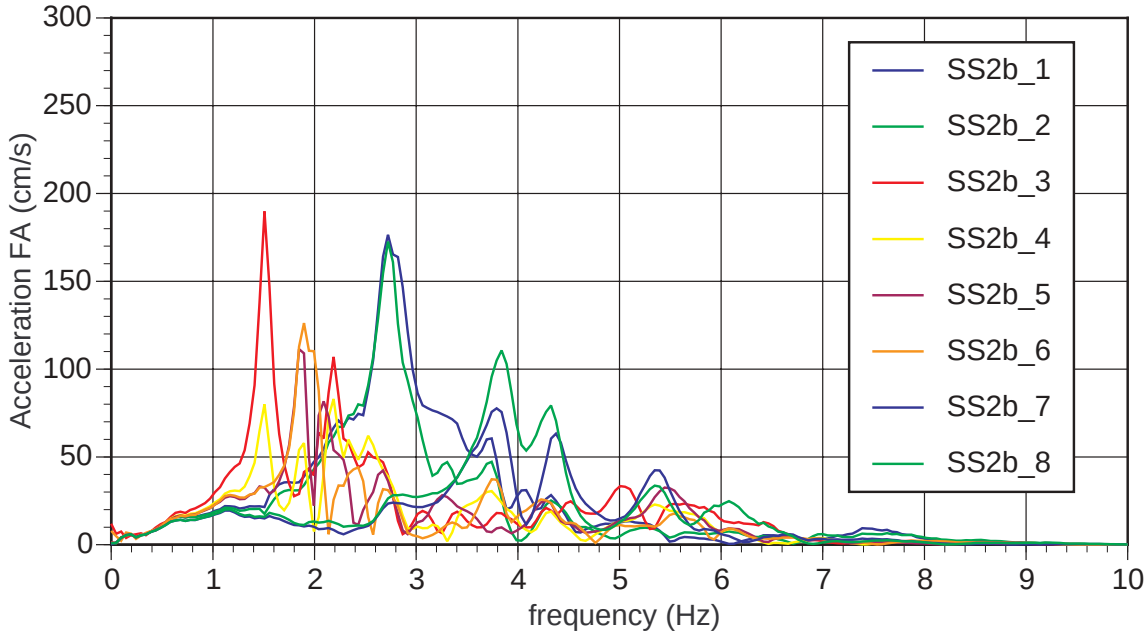

Figure 21. Fourier amplitude spectra of the transverse accelerations calculated at the eight pier sites using the source-section configuration SS2b.

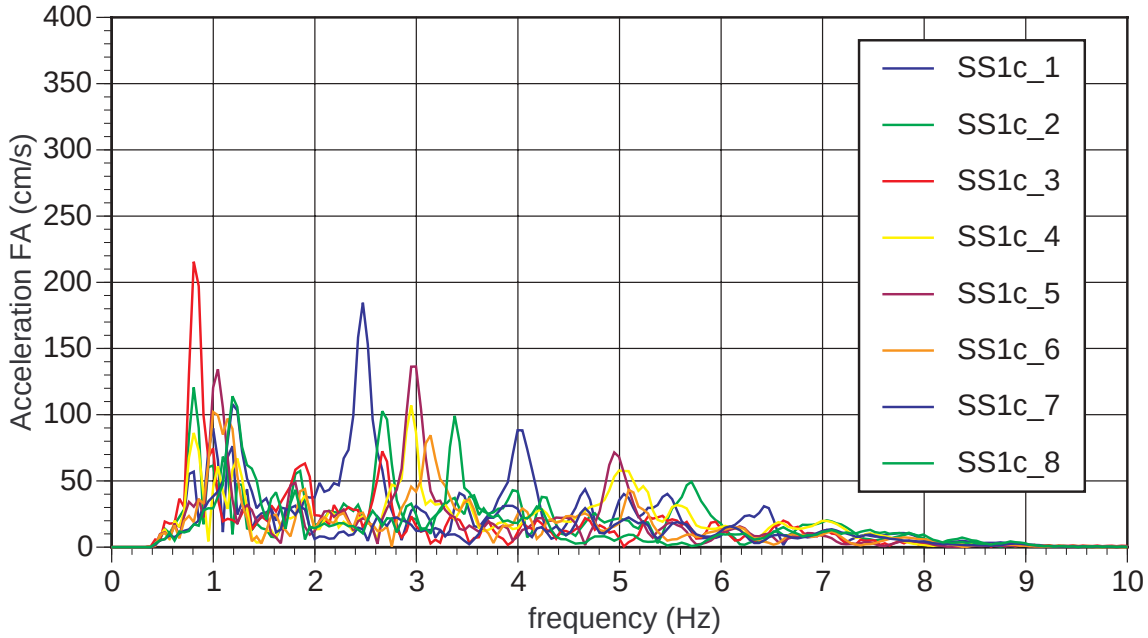

Figure 22. Fourier amplitude spectra of the transverse accelerations calculated at the eight pier sites using the source-section configuration SS1c.

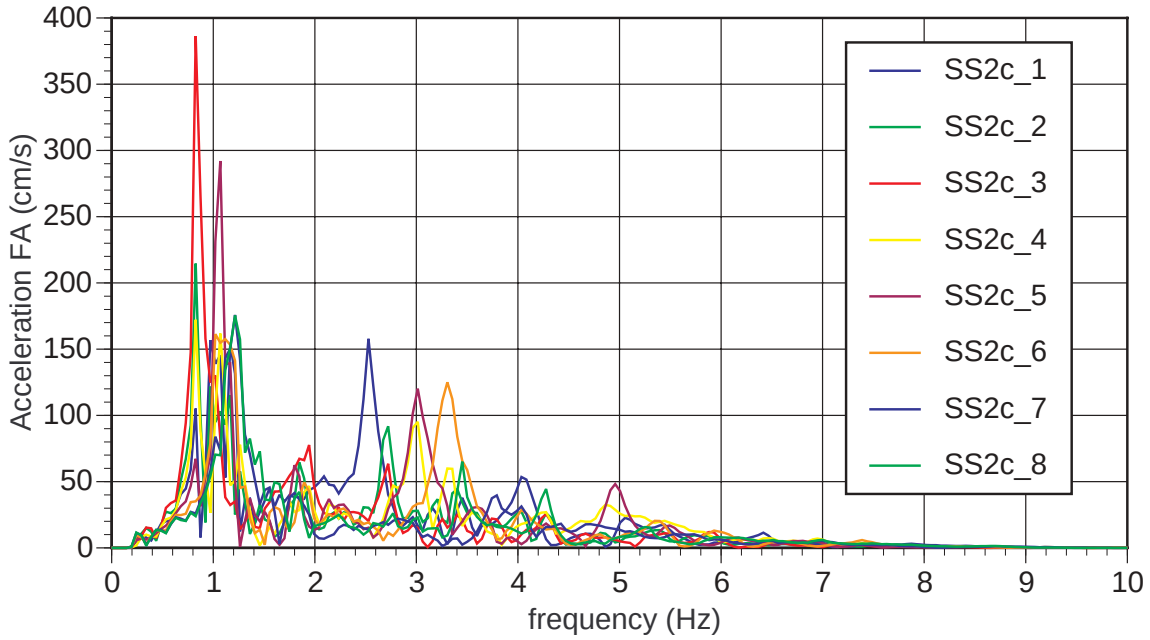

Figure 23. Fourier amplitude spectra of the transverse accelerations calculated at the eight pier sites using the source-section configuration SS2c.

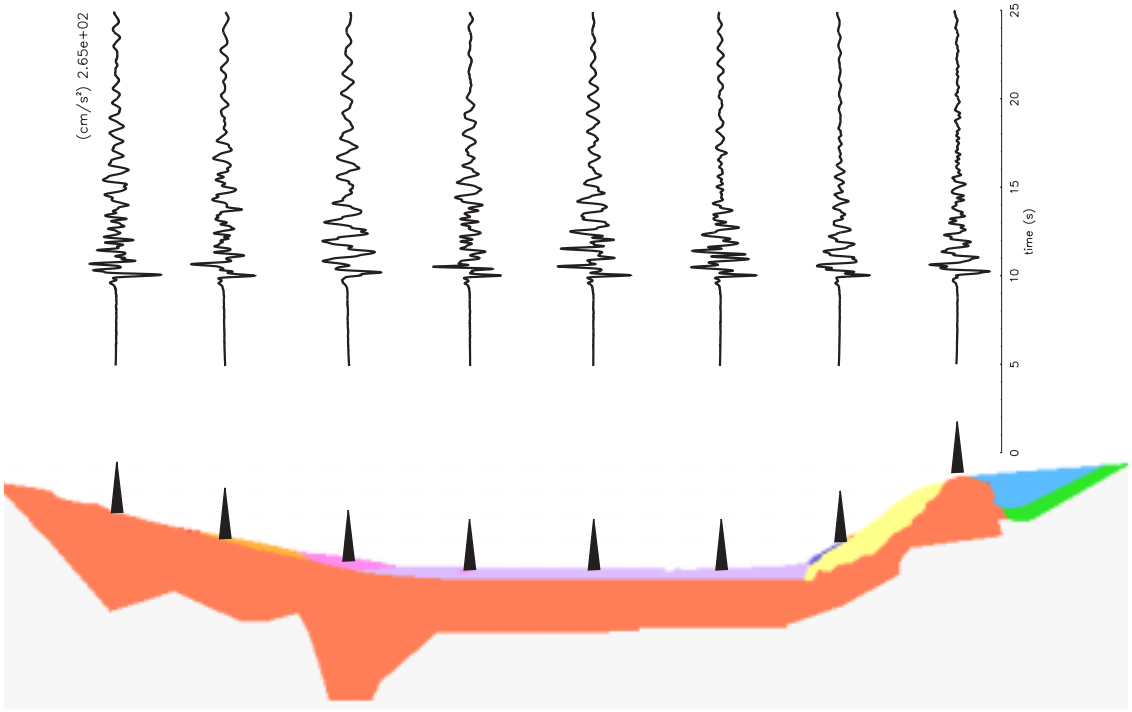

Figure 24. Transverse acceleration time series corresponding to configuration SS2c, calculated at the eight pier sites. The amplitude of the signals is normalized with respect to the maximum one.

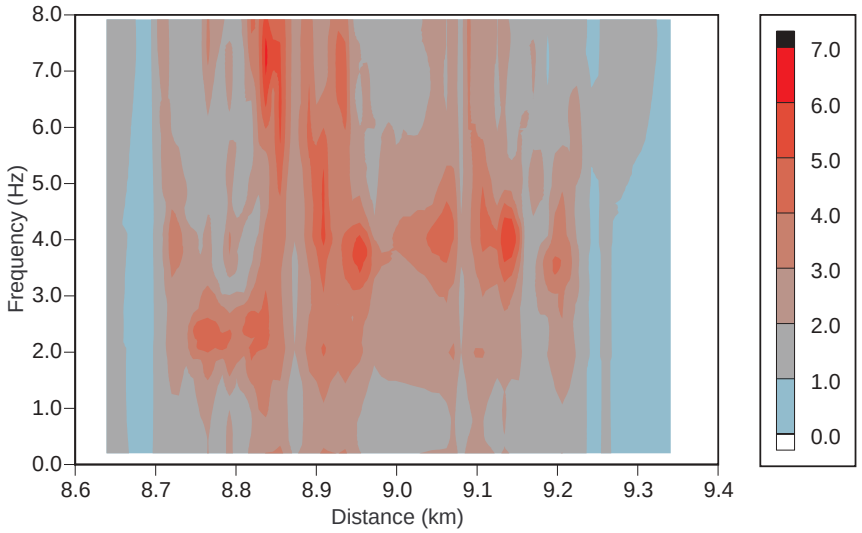

Figure 25. RSR versus epicentral distance and frequency for configuration SS1a.

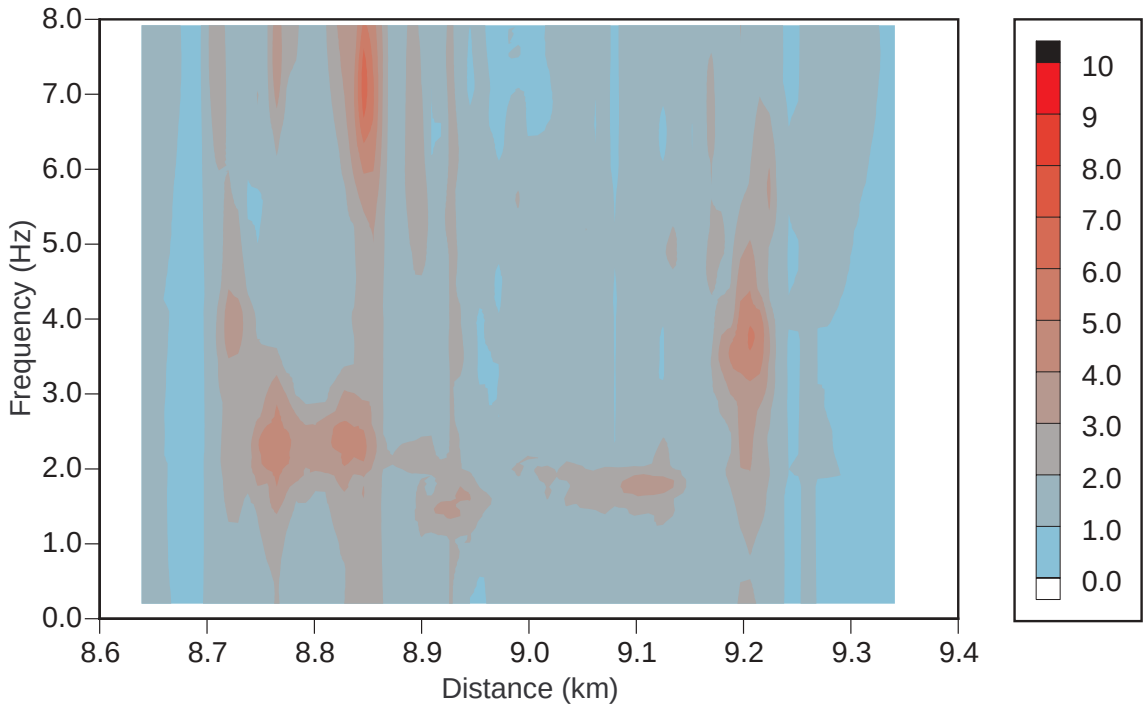

Figure 26. RSR versus epicentral distance and frequency for configuration SS1b.

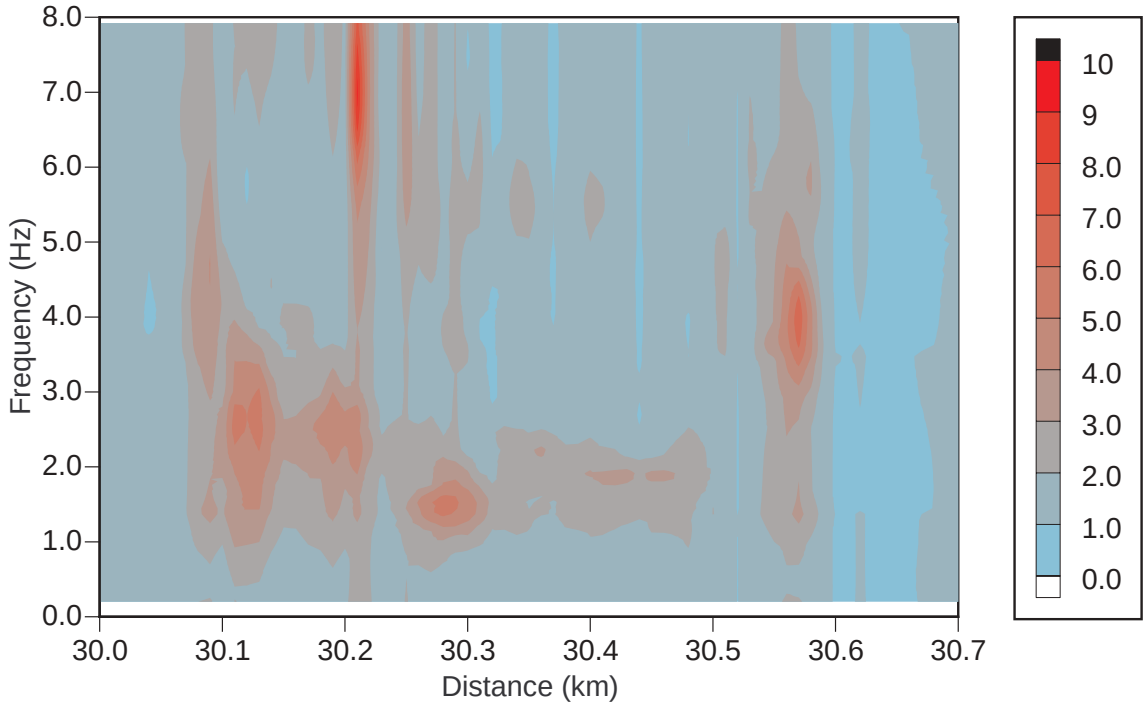

Figure 27. RSR versus epicentral distance and frequency for configuration SS2b.

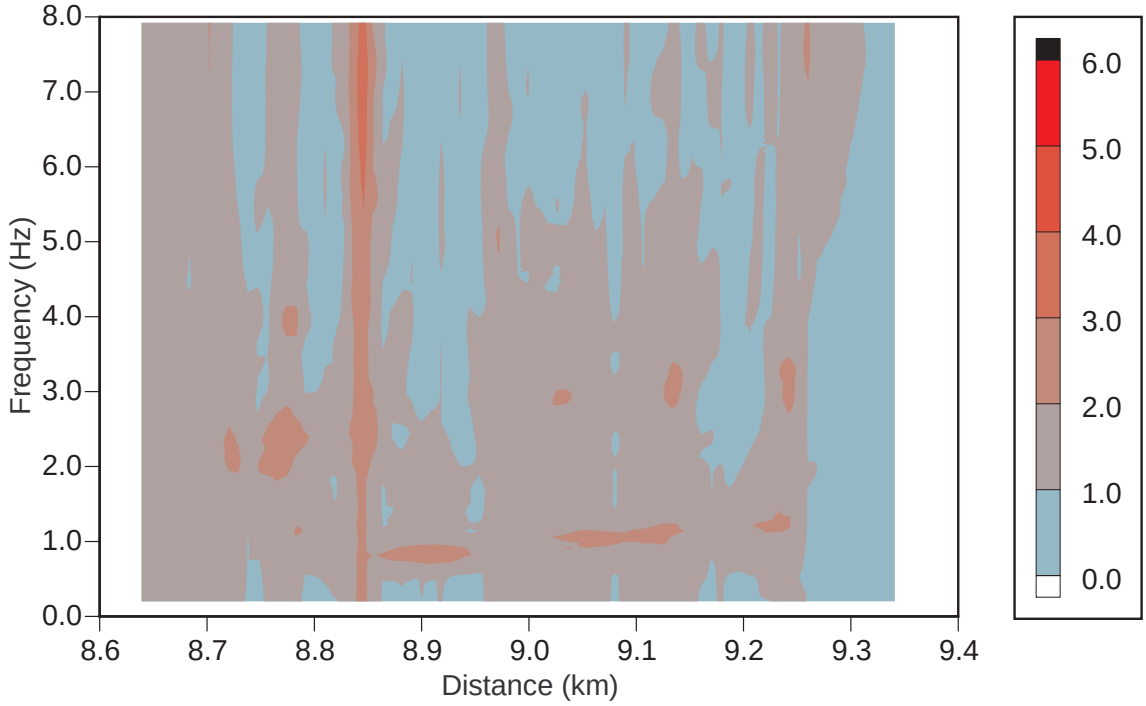

Figure 28. RSR versus epicentral distance and frequency for configuration SS1c.

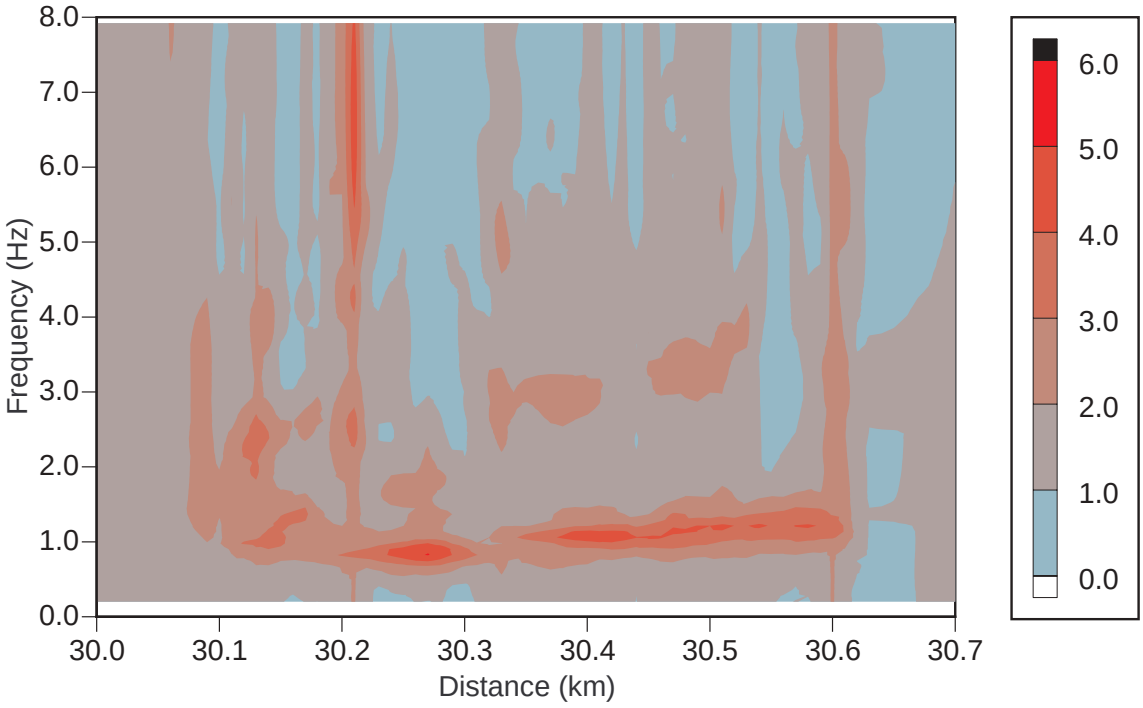

Figure 29. RSR versus epicentral distance and frequency for configuration SS2c.